

Scattering-asymmetry control with ultrafast electron wave packet shaping

Yuya Morimoto^{1,2*}, Peter Hommelhoff² and Lars Bojer Madsen^{3†}

¹ *Ultrashort Electron Beam Science RIKEN Hakubi research team, RIKEN Cluster for Pioneering Research (CPR), RIKEN Center for Advanced Photonics (RAP), 2-1 Hirosawa, Wako, Saitama 351-0198, Japan*

² *Laser Physics, Department of Physics, Friedrich-Alexander-Universität Erlangen-Nürnberg (FAU), Staudtstraße 1, 91058, Erlangen, Germany*

³ *Department of Physics and Astronomy, Aarhus University, 8000 Aarhus C, Denmark*

*yuya.morimoto@riken.jp

†bojer@phys.au.dk

Dated: March 25, 2022.

Scattering of a tightly focused electron beam by an atom forms one of the bases of modern electron microscopy. A fundamental symmetry breaking occurs when the target atom is displaced from the beam center. This displacement results in an asymmetry in the angular distribution of the scattered electrons. Here we propose a concept to control the sign and magnitude of the asymmetry by shaping the incident high-energy electron wave packet in momentum space on the atto- to picosecond time scale. The shaping controls the ultrafast real-space dynamics of the wave packet, shifting the balance between two competing contributions of the impact-parameter-dependent quantum interference and the momentum distribution of the wave packet on the target. We find a strong sensitivity of the scattering on the wave packet properties, an effect that opens promising new avenues for ultrafast electron microscopy.

The conventional theoretical framework describing electron-atom scattering involves a plane-wave description of the incoming projectile electron at large distances as a part of the asymptotic boundary condition [1–3]. This means that the incoming beam is assumed to be infinitely large transversally and of infinite duration longitudinally. In other words, the incident electron is assumed to be monochromatic with a single fixed longitudinal and vanishing transversal momenta. Electron scattering cross sections calculated with these assumptions form the foundation of various research fields [1–3].

In contrast, two recent technical advances allow producing electron beams that cannot be described asymptotically as plane waves. One is the ability to generate a small electron spot. State-of-the-art electron microscopes provide electron beams of sub-Angstrom size [4–8]. In scanning transmission microscopes, atomic-resolution images can be obtained by measuring transmitted or scattered electrons with a probe focused and scanned over the sample. In this case, because of the position-momentum uncertainty, a transversal momentum distribution needs to be considered [9–12]. When the target atom is displaced from the center of the small beam, an asymmetry appears in the angular distribution of the scattered electrons [13,14]. The other notable development is the coherent manipulation of electron beams by light waves [15–25]. Electron pulses as short as hundreds of attoseconds were obtained through temporal compression driven by optical cycles of near- or mid-infrared pulses [17–19,21–25]. The use of optically modulated electron pulses for the efficient excitation of a two-level system [26–29] or coherent photon generation [30–33] were proposed. The confinement of electrons within an extremely short temporal duration is accompanied by a broad longitudinal momentum distribution. If these two techniques, extreme focusing and temporal shaping, are combined, which should be within reach considering the rapid advances of ultrafast electron microscopes [34], a novel regime of electron scattering will open up. However, a comprehensive understanding of scattering of electron wave packets shaped in three-dimensional space is currently lacking.

In this work, we remedy this situation by theoretically investigating fundamental physical quantities, specifically the degree of asymmetry and the total scattering probability, in elastic scattering of electron wave packets shaped in time and space. We consider two types of Gaussian wave packets having atto- to picosecond durations. One has a Gaussian distribution in kinetic energy and the other in the longitudinal momentum. We will show that the two types of wave packets exhibit completely different features when the symmetry of the system is broken due to displacement of the target atom from the beam center. We explain the observations based on quantum-mechanical interference originating from the displaced target and the spatial-momentum overlap between the target and the wave packet occurring on sub-femtosecond time scales. Our findings facilitate the control of the symmetry, strength, phase and timing of electron-

matter interaction by optical electron-beam manipulation in three dimensions. Hence, our work is key for the development of novel imaging techniques in ultrafast electron microscopes.

The physical system under consideration is illustrated in Fig. 1(a). A non-relativistic ultrashort electron wave packet propagating along the z -axis is scattered by a target located at $z = 0$, where the wave packet is transversally focused. The x -axis describes the displacement of the target from the center of the electron beam. Accordingly, the impact parameter is expressed as $\mathbf{b} = b_x \hat{\mathbf{x}}$, where $\hat{\mathbf{x}}$ is the unit vector along the x axis. The momenta of the incident and scattered electrons, $\hbar \mathbf{k}_i$ and $\hbar \mathbf{k}_f$, are described by their absolute values $\hbar k_i$ and $\hbar k_f$, and sets of polar and azimuthal angles (θ_i, φ_i) and (θ_f, φ_f) , see Fig. 1(b). The time-dependent propagating electron wave packet in real space is given by

$$\psi_e(\mathbf{x}, t) = \frac{1}{(2\pi)^{\frac{3}{2}}} \int d\mathbf{k}_i a_e(\mathbf{k}_i) \exp\left(i\mathbf{k}_i \cdot \mathbf{x} - \frac{iE_i t}{\hbar}\right), \quad (1)$$

where $E_i = \hbar^2 k_i^2 / (2m_e)$ is the kinetic energy and $a_e(\mathbf{k}_i)$ is a complex amplitude describing the momentum distribution. The scattering probability is derived from the time-dependent S -matrix theory [35,36]. By employing the first Born approximation and neglecting the exchange interaction, both of which are valid for high-energy electrons (10 keV in this work), the elastic scattering probability is obtained as [36]

$$P(\hat{\mathbf{k}}_f, \mathbf{b}) = P_0 \int k_i^3 dk_i \iint d\hat{\mathbf{k}}_i \iint d\hat{\mathbf{k}}'_i \\ \times a_e^*(k_i, \hat{\mathbf{k}}'_i) a_e(k_i, \hat{\mathbf{k}}_i) T_{\text{el}}^*(k_i, \hat{\mathbf{k}}'_i, \hat{\mathbf{k}}_f) T_{\text{el}}(k_i, \hat{\mathbf{k}}_i, \hat{\mathbf{k}}_f) e^{ik_i(\hat{\mathbf{k}}_i - \hat{\mathbf{k}}'_i) \cdot \mathbf{b}}, \quad (2)$$

where $\hat{\mathbf{k}}_i = \mathbf{k}_i/k_i$, $\hat{\mathbf{k}}'_i = \mathbf{k}'_i/k_i$, $\hat{\mathbf{k}}_f = \mathbf{k}_f/k_f$ with $k_f = k_i$, and P_0 a constant. Equation (2) shows that the scattering probability contains a coherent contribution from two scattering pathways, from \mathbf{k}_i to \mathbf{k}_f and \mathbf{k}'_i to \mathbf{k}_f . T_{el} in Eq. (2) is the first Born scattering amplitude, i.e., the atomic form factor. In this work, for simplicity, we consider the target to be atomic hydrogen in the 1s state. The atomic form factor is thus given by $T_{\text{el}}(q) = T_0 a_0^2 (a_0^2 q^2 + 8) / (a_0^2 q^2 + 4)^2$ [1], where $\hbar \mathbf{q} = \hbar k_i (\hat{\mathbf{k}}_i - \hat{\mathbf{k}}_f)$ is the momentum transfer, a_0 the Bohr radius and T_0 a real-valued constant.

We consider two types of axially-symmetric 10-keV electron-beam wave packets. The axial symmetry allows us to describe the momentum-space wavefunction $a_e(\mathbf{k}_i)$ by (k_i, θ_i) . Their momentum-space densities are sketched in Fig. 1(d). The first one (right side) is defined as

$$a_e(k_i, \theta_i) = \frac{1}{(32\pi^3)^{\frac{1}{4}} \sqrt{\sigma_{\parallel} \sigma_{\theta}}} \exp\left(-\frac{(k_{\parallel} - k_e)^2}{4\sigma_{\parallel}^2}\right) \exp\left(-\frac{\sin^2 \theta_i}{4\sigma_{\theta}^2}\right), \quad (3)$$

where $k_{\parallel} = k_i \cos \theta_i$ is the longitudinal momentum, k_e the total momentum for 10-keV electrons, and $\hbar\sigma_{\parallel}$ the root-mean-square (rms) longitudinal momentum width. In real space, the rms longitudinal size can be as small as $1/(2\sigma_{\parallel})$ and the corresponding FWHM duration is $\tau = \sqrt{2 \ln(2)}/(\sigma_{\parallel} v_e)$. σ_{θ} is the rms angular width and throughout this work, we use $\sigma_{\theta} = 10$ mrad, a typical value for transmission electron microscopes [37]. The corresponding rms spot size is $1/(2k_e \sigma_{\theta}) = 1 \text{ \AA}$. Since this wave packet has a Gaussian distribution in the longitudinal momentum, we call it a k_{\parallel} -Gauss wave packet. The wavefunction is normalized, $\int |a_e(k_i, \theta_i)|^2 d\mathbf{k}_i = 1$.

The second wave packet [left side of Fig. 1(d)] is defined as

$$a_e(k_i, \theta_i) = \frac{1}{(32\pi^3)^{\frac{1}{4}} \sqrt{\sigma_{\parallel}} \sigma_{\theta}} \exp\left(-\frac{(k_i - k_e)^2}{4\sigma_{\parallel}^2}\right) \exp\left(-\frac{\sin^2 \theta_i}{4\sigma_{\theta}^2}\right). \quad (4)$$

Since this wave packet has a Gaussian distribution in the total momentum k_i , we call it a $|k|$ -Gauss wave packet. In the limit $\sigma_{\parallel} \rightarrow +0$ (i.e., $\tau \rightarrow +\infty$), this wave packet resembles the monochromatic but transversally focused beams in electron microscopes. In the limit $\sigma_{\parallel} \rightarrow +\infty$ (i.e., $\tau \rightarrow +0$), the above two types of wave packets are nearly identical. The two wave-packet types can be produced with existing experimental techniques as discussed in the Supplemental Material [38]. We consider wave packet durations τ in the range from 1 as to 1 ps.

The two, colored circles in Fig. 1(a) show azimuthal (φ_f) contrasts $C_{\varphi}(\theta_f, \varphi_f, b_x)$ calculated for the two wave packet types with $\tau = 1$ fs and $b_x = 3 \text{ \AA}$. The contrast is defined by $C_{\varphi}(\theta_f, \varphi_f, b_x) = P(\theta_f, \varphi_f, b_x)/P_{\text{ave}}(\theta_f, b_x) - 1$ where $P_{\text{ave}}(\theta_f, b_x) = \int_0^{2\pi} P(\theta_f, \varphi_f, b_x) d\varphi_f / (2\pi)$ is the scattering probability averaged over the azimuthal angle φ_f . In these circles, the radius corresponds to the scattering angle (θ_f). We observe an asymmetry with a 2-fold (180°) periodicity in $C_{\varphi}(\theta_f, \varphi_f, b_x)$ and, most importantly, the sign of the asymmetry is opposite for the two wave packet types. The $|k|$ -Gauss wave packet (left) shows lower (red) scattering probabilities along the direction of the target while the k_{\parallel} -Gauss wave packet (right) shows higher (blue) probabilities. We introduce the asymmetry parameter for the quantitative discussion below,

$$A_{\varphi}(b_x) = \frac{\int \{P(\theta_f, \varphi_f = 0, b_x) - P(\theta_f, \varphi_f = \pi/2, b_x)\} \sin \theta_f d\theta_f}{P_{\text{total}}/(2\pi)}, \quad (5)$$

where $P_{\text{total}}(b_x) = \iint P(\theta_f, \varphi_f, b_x) \sin \theta_f d\theta_f d\varphi_f$ in the denominator is the total scattering probability. A positive value of $A_{\varphi}(b_x)$ represents a higher probability for $\varphi_f = 0$ than for $\varphi_f = \pi/2$.

Figure 2 compares the total scattering probabilities (upper panels) $P_{\text{total}}(b_x)$ and the azimuthal asymmetry $A_\varphi(b_x)$ (lower panels) for the two types of wave packets as a function of their duration τ . We consider impact parameters b_x from 0 Å to 5 Å. The $|k|$ -Gauss wave packet (left) results in a scattering probability nearly independent of the wave-packet duration. However, the impact parameter dependence is significant: the scattering probability at $b_x = 5$ Å is six orders of magnitude lower than that at $b_x = 0$ Å with a beam of ~ 1 Å rms spot size. This high contrast provides the ability to probe atoms with high spatial resolution, which is the physical background of the atomic-resolution scanning transmission microscopy [37,39]. The azimuthal asymmetry A_φ [left panel of Fig. 2(b)] is always negative and nearly independent of the wave-packet duration. As expected, the degree of asymmetry increases with impact parameter.

In contrast, the scattering probability and the azimuthal asymmetry of the $k_{||}$ -Gauss wave packet (right panels) strongly depend on the wave-packet duration τ . For this pulsed beam, we identified three regimes. At very short durations of $\tau < 0.1$ fs, the results are nearly identical to those of the $|k|$ -Gauss (left panels). This is because the two types of wave packets cannot be distinguished in the limit $\sigma_{||} \rightarrow +\infty$ (i.e., $\tau \rightarrow +0$). At the transient regime from 0.1 fs to 10 fs, the scattering probability and the asymmetry drastically changes, especially for the larger impact parameters considered. The sign of the asymmetry even flips. In the long duration regime ($\tau > 10$ fs), the scattering probability decreases monotonically, while the asymmetry is positive and almost constant.

In order to gain a physical understanding of these findings, we first consider the spatial distributions of the wave packets and relate them to the scattering probabilities. Figure 3(a) shows snapshots of the probability densities $|\psi_e(x, y = 0, z, t)|^2$ in the xz plane for a duration of $\tau = 1$ fs, evolving on sub-femtosecond time scales. At $t = 0$ fs (lowest panels), the wave packets are spatially focused. The upper panels show the real-space densities at negative times (i.e., before the focus). The overall density distribution of the $|k|$ -Gauss wave packet (left panels) follows the shape of a focused Gaussian beam known from optics [40]. The overall shape does not change with the wave-packet duration (not shown), suggesting the independence of the scattering probabilities on the packet duration (left panels of Fig. 2). Figure 3(b) shows the temporal evolution of the wave-packet densities at $z = 0$ [vertical slices of Fig. 3(a)], where the target atom is placed. The probability densities are peaked at around $x = 0$. This leads to the observed significant decay of the scattering probability with the impact parameter.

On the other hand, the real-space densities of the $k_{||}$ -Gauss wave packet [right panels of Fig. 3(a)] have a two-dimensional Gaussian shape at any time. Interestingly, we find non-negligible densities at large x and $z = 0$ (vertical lines), at the times of -1.0 fs and -0.5 fs. The right panel of Fig. 3(b) shows the temporal

evolution of the densities at $z = 0$. Noteworthy, at a large x , there are two density peaks in time, separated by 0.9 fs at $x = 5 \text{ \AA}$ (green curve in lower panel), whose potential applications will be briefly discussed in the concluding remarks. Because the longitudinal size is determined by the wave-packet duration τ , the amount of the overlap with the target at larger x are strongly affected by τ . The illustrations in Fig. 4(a) qualitatively explain the dependence on τ . The blue elliptical circles show the spatial distribution of the wave packets at $t = 0$. From each point of the wave packet, the electron spreads with a given divergence angle (arrows). At a very short duration (left), even a large spreading angle component does not cross the target atom. At an intermediate duration (middle), a large-angle component starting from the edge of the distribution traverses the target. At a very long duration (right), components from small to large angles can cross the target but the contribution of each component is small because the wave packet is extended along z . Accordingly, the scattering probability decreases with $\sim 1/\tau$ [right panel of Fig. 2(a)]. The wave-packet duration corresponding to the intermediate regime for $b_x = 5 \text{ \AA}$ can be estimated as $b_x/(\sigma_\theta v_e/2) \sim 0.8 \text{ fs}$, see the middle panel of Fig. 4(a).

In order to quantitatively confirm the above discussion, we simulated time-integrated probability densities at $y = z = 0$, that is $\int_{-\infty}^{+\infty} |\psi_e(x, y = 0, z = 0, t)|^2 dt$, for the two types of the wave packets. Circles in Fig. 2(a) show such densities at $x = b_x$. For the comparison, the densities are normalized using the scattering probabilities at $b_x = 0 \text{ \AA}$ and $\tau = 0.01 \text{ fs}$. We obtain good matches between the probability densities (circles) and the scattering probabilities (curves) for both wave packets. Even the curves with complicated shapes for the $k_{//}$ -Gauss wave packet (right panel) are reproduced well. The good agreement validates the physical picture of Fig. 4(a) and confirms the connection between the local probability density and the scattering probability. At points of very small ($< 10^{-2}$) scattering probabilities, the local densities underestimate the scattering probabilities. This discrepancy could originate from the long-range nature of the Coulomb potential of the target atom.

The physical picture in Fig. 4(a) also explains the positive azimuthal asymmetry $A_\phi(b_x)$ seen in the right panel of Fig 2(b). Intuitively, components with transversal momenta along x can likely reach the target compared to those along y (perpendicular to the plane). This can produce an anisotropy in the (k_x, k_y) distribution of electrons coming to the target. Because the scattering probability is higher with smaller momentum transfer $|\hbar\mathbf{q}|$ [see expression for $T_{\text{el}}(q)$ after Eq. (2)], this anisotropy is translated into the angular distribution of scattered electrons, leading to the azimuthal asymmetry. We quantify the momentum anisotropy by using the Gabor transform as

$$Q(x, y, z, k_x, k_y) = \iint dt dk_z |G(x, y, z, k_x, k_y, k_z, t)|^2, \quad (6)$$

with

$$G(x, y, z, k_x, k_y, k_z, t) = \frac{1}{(2\pi)^{\frac{3}{2}}} \iiint \psi_e(x', y', z', t) \exp\left(-\frac{(x'-x)^2}{2\delta_x^2}\right) \exp\left(-\frac{(y'-y)^2}{2\delta_y^2}\right) \exp\left(-\frac{(z'-z)^2}{2\delta_z^2}\right) \times \exp(-ik_x x') \exp(-ik_y y') \exp(-ik_z z') dx' dy' dz', \quad (7)$$

where $\delta_x, \delta_y, \delta_z$ are the rms spatial width of interests. Equations (6) and (7) show that the Gabor transform extracts information on the momentum density distributions (k_x, k_y, k_z) of the wave packet at the position of the target (x, y, z) . Figure 4(b) shows the two-dimensional momentum distribution $Q(x, y, z, k_x, k_y)$ of the k_{\parallel} -Gauss wave packet at $x = 5 \text{ \AA}, y = z = 0 \text{ \AA}$ for packet durations $\tau = 0.1 \text{ fs}$ (left), 1 fs (middle) and 10 fs (right). We chose a relatively large value of $\delta_x = \delta_y = \delta_z = 2 \text{ \AA}$ in order to see their differences clearly. At the short duration of 0.1 fs , the momentum distribution is isotropic. On the other hand, at $\tau = 1 \text{ fs}$, the distribution is significantly anisotropic and there are two peaks at $k_x \sim \pm 0.7 \text{ \AA}^{-1}$. At $\tau = 10 \text{ fs}$, the k_x - k_y anisotropy is reduced but not lost. This trend matches with the physical picture of Fig. 4(a) and explains the results in the right panel of Fig. 2(b), where the azimuthal asymmetry peaks at hundreds of attoseconds, and decreases at longer durations. Based on these results, we conclude that the positive azimuthal asymmetry, i.e., stronger scattering probabilities towards/against the target direction ($\varphi_f = 0, \pi$), for the k_{\parallel} -Gauss wave packet is attributed to the anisotropic momentum distribution given by the real-space wave-packet dynamics on few-femtosecond time scales.

Finally, we explain the origin of the negative azimuthal asymmetry appearing in the scattering of the $|k|$ -Gauss wave packet and the short-duration k_{\parallel} -Gauss wave packet [see Fig. 2(a)]. We return to Eq. (2) and focus on the term $e^{ik_i(\hat{\mathbf{k}}_i - \hat{\mathbf{k}}'_i) \cdot \mathbf{b}}$. The physical origin of this phase term is illustrated in Fig. 1(c). For an electron with an incident angle θ_i on the xz plane, one can find the difference in the geometrical path length as compared to the case of $b_x = 0$, which is given by $\hat{\mathbf{k}}_i \cdot \mathbf{b} = b_x \sin \theta_i$, shown by the red arrow. Note that a similar discussion is applied to electron diffraction by molecules or crystals. The scattering probability in Eq. (2) contains the relative phase for \mathbf{k}_i and \mathbf{k}'_i , that is $e^{ik_i(\hat{\mathbf{k}}_i - \hat{\mathbf{k}}'_i) \cdot \mathbf{b}}$. Because smaller momentum transfer $|\hbar\mathbf{q}|$ leads to higher scattering probabilities, the scattering to $\varphi_f = 0$ and π can be represented by that occurring on the xz plane, in which the phase term is given by $e^{ik_i(\sin \theta_i - \sin \theta'_i) \cdot b_x}$, while the scattering to $\varphi_f = \pi/2$ and $3\pi/2$ can be represented by an event on the yz plane, in which the phase term is $e^0 = 1$ because $\hat{\mathbf{k}}_i$ and $\hat{\mathbf{k}}'_i$ are perpendicular to \mathbf{b} . Therefore, the term inside the integral of Eq. (2) is added in phase for the scattering on the yz plane, leading to the higher scattering probabilities at $\varphi_f = \pi/2, 3\pi/2$ than at $\varphi_f = 0, \pi$.

In summary, motivated by the rapid advances on light-driven control of electron beams, we investigated the fundamental aspects of scattering of electron wave packets shaped in 3D space. The

dependence of the scattering probabilities on the wave-packet type, duration and impact parameters were elucidated by the spatial-momentum overlap between the incident beam with the target atom occurring on the few-femtosecond time scale. The two types of ultrashort wave packets considered in this work can be used for the atomic-resolution electron microscopy when appropriately shaped and focused. The azimuthal asymmetry induced by the displacement of the target from the electron beam center is attributed to two competing effects, the anisotropy of momentum distribution, which was revealed by the Gabor transform, and the geometrical phase determined by the impact parameter. Both the scattering probability and asymmetry related to the use of the wave packet with a Gaussian distribution in the longitudinal momentum strongly depend on its duration in the range of 0.01-100 fs, further suggesting a novel *in-situ* approach to characterize the temporal duration of the ultrashort wave packet in an extreme temporal parameter range purely from time-unresolved scattering data. Moreover, the target displaced from the beam center experiences two electron bursts within a single wave packet [right panel of Fig. 3(b)] whose separation is tunable with the displacement distance on the few-femtosecond time scale level (0.5 fs at $b_x = 3 \text{ \AA}$ and 0.9 fs at $b_x = 5 \text{ \AA}$), which could be useful for coherently exciting the target through the free-electron—bound electron transition scheme [26,27], probing the electronic coherence of the atom [29,41], or for an electron-pump--electron-probe experiment of sub-femtosecond carrier dynamics.

ACKNOWLEDGEMENTS

This work is supported by the Japan Science and Technology Agency through ACT-X Grant Number JPMJAX21AO, the Research Foundation for Opto-Science and Technology, the Gordon and Betty Moore Foundation (GBMF) through Grant No. GBMF4744 “Accelerator on a Chip International Program-ACHIP”, ERC Advanced Grant No. 884217 “AccelOnChip” and the Independent Research Fund Denmark (GrantNo.9040-00001B and 1026-00040B).

- [1] N. F. Mott and H. S. W. Massey, *The Theory of Atomic Collisions* (Clarendon Press, Oxford, 1965).
- [2] Roger G. Newton, *Scattering Theory of Waves and Particles* (Dover Publications, New York, 2002).
- [3] Goldberger M.L. and Watson K. M., *Collision Theory* (John Wiley & Sons, New York, 1964).
- [4] N. Shibata, S. D. Findlay, Y. Kohno, H. Sawada, Y. Kondo, and Y. Ikuhara, *Differential Phase-Contrast Microscopy at Atomic Resolution*, Nat. Phys. **8**, 611 (2012).
- [5] K. Müller, F. F. Krause, A. Béch e, M. Schowalter, V. Galioit, S. Löffler, J. Verbeeck, J. Zweck, P. Schattschneider, and A. Rosenauer, *Atomic Electric Fields Revealed by a Quantum Mechanical Approach to Electron Picodiffraction*, Nat. Commun. **5**, (2014).
- [6] N. Shibata, T. Seki, G. Sánchez-Santolino, S. D. Findlay, Y. Kohno, T. Matsumoto, R. Ishikawa,

- and Y. Ikuhara, *Electric Field Imaging of Single Atoms*, Nat. Commun. **8**, 15631 (2017).
- [7] Y. Kohno, T. Seki, S. D. Findlay, Y. Ikuhara, and N. Shibata, *Real-Space Visualization of Intrinsic Magnetic Fields of an Antiferromagnet*, Nature **602**, 234 (2022).
- [8] R. Erni, M. D. Rossell, C. Kisielowski, and U. Dahmen, *Atomic-Resolution Imaging with a Sub-50-pm Electron Probe*, Phys. Rev. Lett. **102**, 096101 (2009).
- [9] R. Close, Z. Chen, N. Shibata, and S. D. Findlay, *Towards Quantitative, Atomic-Resolution Reconstruction of the Electrostatic Potential via Differential Phase Contrast Using Electrons*, Ultramicroscopy **159**, 124 (2015).
- [10] K. Müller-Caspary, F. F. Krause, T. Grieb, S. Löffler, M. Schowalter, A. Béché, V. Galioit, D. Marquardt, J. Zweck, P. Schattschneider, J. Verbeeck, and A. Rosenauer, *Measurement of Atomic Electric Fields and Charge Densities from Average Momentum Transfers Using Scanning Transmission Electron Microscopy*, Ultramicroscopy **178**, 62 (2017).
- [11] T. Seki, G. Sánchez-Santolino, R. Ishikawa, S. D. Findlay, Y. Ikuhara, and N. Shibata, *Quantitative Electric Field Mapping in Thin Specimens Using a Segmented Detector: Revisiting the Transfer Function for Differential Phase Contrast*, Ultramicroscopy **182**, 258 (2017).
- [12] M. C. Cao, Y. Han, Z. Chen, Y. Jiang, K. X. Nguyen, E. Turgut, G. D. Fuchs, and D. A. Muller, *Theory and Practice of Electron Diffraction from Single Atoms and Extended Objects Using an EMPAD*, Microscopy **67**, i150 (2018).
- [13] D. V. Karlovets, G. L. Kotkin, and V. G. Serbo, *Scattering of Wave Packets on Atoms in the Born Approximation*, Phys. Rev. A **92**, 052703 (2015).
- [14] D. V. Karlovets, G. L. Kotkin, V. G. Serbo, and A. Surzhykov, *Scattering of Twisted Electron Wave Packets by Atoms in the Born Approximation*, Phys. Rev. A **95**, 032703 (2017).
- [15] C. Kealhofer, W. Schneider, D. Ehberger, A. Ryabov, F. Krausz, and P. Baum, *All-Optical Control and Metrology of Electron Pulses*, Science **352**, 429 (2016).
- [16] D. Zhang, A. Fallahi, M. Hemmer, X. Wu, M. Fakhari, Y. Hua, H. Cankaya, A.-L. Calendron, L. E. Zapata, N. H. Matlis, and F. X. Kärtner, *Segmented Terahertz Electron Accelerator and Manipulator (STEAM)*, Nat. Photonics **12**, 336 (2018).
- [17] Y. Morimoto and P. Baum, *Single-Cycle Optical Control of Beam Electrons*, Phys. Rev. Lett. **125**, 193202 (2020).
- [18] Y. Morimoto and P. Baum, *Diffraction and Microscopy with Attosecond Electron Pulse Trains*, Nat. Phys. **14**, 252 (2018).
- [19] K. E. Priebe, C. Rathje, S. V. Yalunin, T. Hohage, A. Feist, S. Schäfer, and C. Ropers, *Attosecond Electron Pulse Trains and Quantum State Reconstruction in Ultrafast Transmission Electron Microscopy*, Nat. Photonics **11**, 793 (2017).
- [20] D. Ehberger, K. J. Mohler, T. Vasileiadis, R. Ernstorfer, L. Waldecker, and P. Baum, *Terahertz Compression of Electron Pulses at a Planar Mirror Membrane*, Phys. Rev. Appl. **11**, 024034 (2019).
- [21] C. M. S. Sears, E. Colby, R. Ischebeck, C. McGuinness, J. Nelson, R. Noble, R. H. Siemann, J. Spencer, D. Walz, T. Plettner, and R. L. Byer, *Production and Characterization of Attosecond Electron Bunch Trains*, Phys. Rev. Spec. Top. - Accel. Beams **11**, 061301 (2008).
- [22] M. Kozák, N. Schönenberger, and P. Hommelhoff, *Ponderomotive Generation and Detection of Attosecond Free-Electron Pulse Trains*, Phys. Rev. Lett. **120**, 103203 (2018).
- [23] N. Schönenberger, A. Mittelbach, P. Yousefi, J. McNeur, U. Niedermayer, and P. Hommelhoff, *Generation and Characterization of Attosecond Microbunched Electron Pulse Trains via Dielectric Laser Acceleration*, Phys. Rev. Lett. **123**, 264803 (2019).
- [24] D. S. Black, U. Niedermayer, Y. Miao, Z. Zhao, O. Solgaard, R. L. Byer, and K. J. Leedle, *Net Acceleration and Direct Measurement of Attosecond Electron Pulses in a Silicon Dielectric Laser Accelerator*, Phys. Rev. Lett. **123**, 264802 (2019).
- [25] U. Niedermayer, D. S. Black, K. J. Leedle, Y. Miao, R. L. Byer, and O. Solgaard, *Low-Energy-Spread Attosecond Bunching and Coherent Electron Acceleration in Dielectric Nanostructures*, Phys. Rev. Appl. **15**, L021002 (2021).

- [26] L. D. Favro, D. M. Fradkin, and P. K. Kuo, *Energy Transfer via Scattering of a Coherent Modulated Electron Beam*, Phys. Rev. D **3**, 2934 (1971).
- [27] A. Gover and A. Yariv, *Free-Electron–Bound-Electron Resonant Interaction*, Phys. Rev. Lett. **124**, 064801 (2020).
- [28] D. Rätzel, D. Hartley, O. Schwartz, and P. Haslinger, *Controlling Quantum Systems with Modulated Electron Beams*, Phys. Rev. Res. **3**, 023247 (2021).
- [29] Z. Zhao, X.-Q. Sun, and S. Fan, *Quantum Entanglement and Modulation Enhancement of Free-Electron–Bound-Electron Interaction*, Phys. Rev. Lett. **126**, 233402 (2021).
- [30] Y. Pan and A. Gover, *Spontaneous and Stimulated Emissions of a Preformed Quantum Free-Electron Wave Function*, Phys. Rev. A **99**, 052107 (2019).
- [31] A. Karnieli, N. Rivera, A. Arie, and I. Kaminer, *The Coherence of Light Is Fundamentally Tied to the Quantum Coherence of the Emitting Particle*, Sci. Adv. **7**, abf8096 (2021).
- [32] O. Kfir, V. Di Giulio, F. J. G. de Abajo, and C. Ropers, *Optical Coherence Transfer Mediated by Free Electrons*, Sci. Adv. **7**, abf6380 (2021).
- [33] V. Di Giulio, O. Kfir, C. Ropers, and F. J. García de Abajo, *Modulation of Cathodoluminescence Emission by Interference with External Light*, ACS Nano **15**, 7290 (2021).
- [34] A. H. Zewail and J. M. Thomas, *4D Electron Microscopy: Imaging in Space and Time*. (World Scientific, Singapore, 2009).
- [35] H.-C. Shao and A. F. Starace, *Imaging Coherent Electronic Motion in Atoms by Ultrafast Electron Diffraction*, Phys. Rev. A **88**, 062711 (2013).
- [36] Y. Morimoto, P. Hommelhoff, and L. B. Madsen, *Coherent Scattering of an Optically Modulated Electron Beam by Atoms*, Phys. Rev. A **103**, 043110 (2021).
- [37] D. B. Williams and C. B. Carter, *Transmission Electron Microscopy* (Springer US, Boston, MA, 2009).
- [38] See Supplemental Material, [URL], for potential experimental approaches to obtain the electron wave packets discussed in this work.
- [39] S. J. Pennycook and P. D. Nellist, *Scanning Transmission Electron Microscopy* (Springer, New York, 2011).
- [40] M. Born and E. Wolf, *Principles of Optics* (Cambridge University Press, Cambridge, 1999).
- [41] R. Ruimy, A. Gorlach, C. Mechel, N. Rivera, and I. Kaminer, *Toward Atomic-Resolution Quantum Measurements with Coherently Shaped Free Electrons*, Phys. Rev. Lett. **126**, 233403 (2021).
- [42] L. Zhang, J. P. Hoogenboom, B. Cook, and P. Kruit, *Photoemission Sources and Beam Blankers for Ultrafast Electron Microscopy*, Struct. Dyn. **6**, 051501 (2019).
- [43] Y. Morimoto and P. Baum, *Attosecond Control of Electron Beams at Dielectric and Absorbing Membranes*, Phys. Rev. A **97**, 033815 (2018).

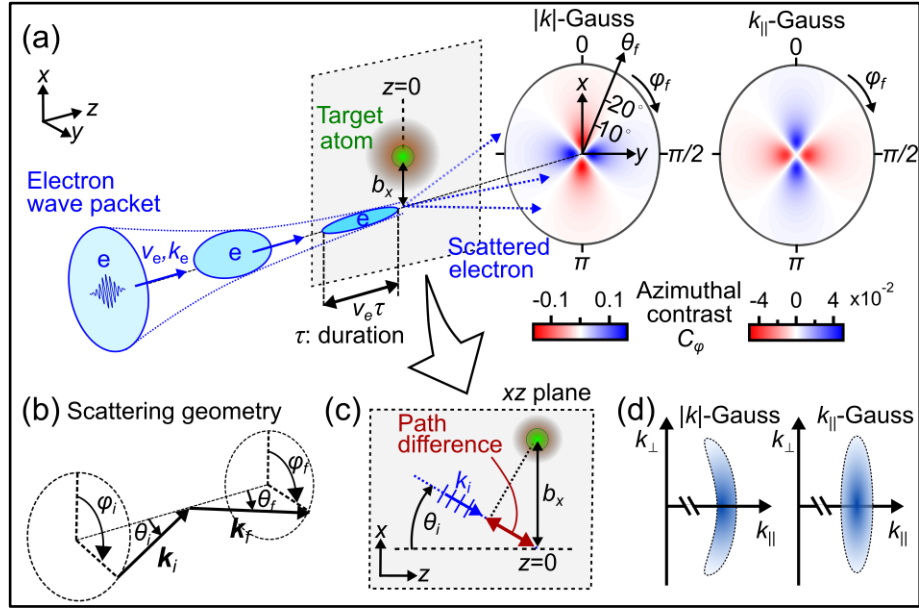


Fig 1. Scattering of a 3D-shaped ultrashort electron wave packet. (a) Concept and physical system. The spatially focused electron pulse is scattered by a target (atomic hydrogen) displaced from the beam center. An azimuthal asymmetry appears in the angular distribution of the scattered electrons (right circles). The right circles show the azimuthal contrast on a two-dimensional detector. (b) Scattering geometry. (c) Illustration of the geometrical path length difference, leading to the b -dependent phase of Eq. (2). (d) Sketches of the momentum distributions of the considered ultrashort wave packets. See text for details.

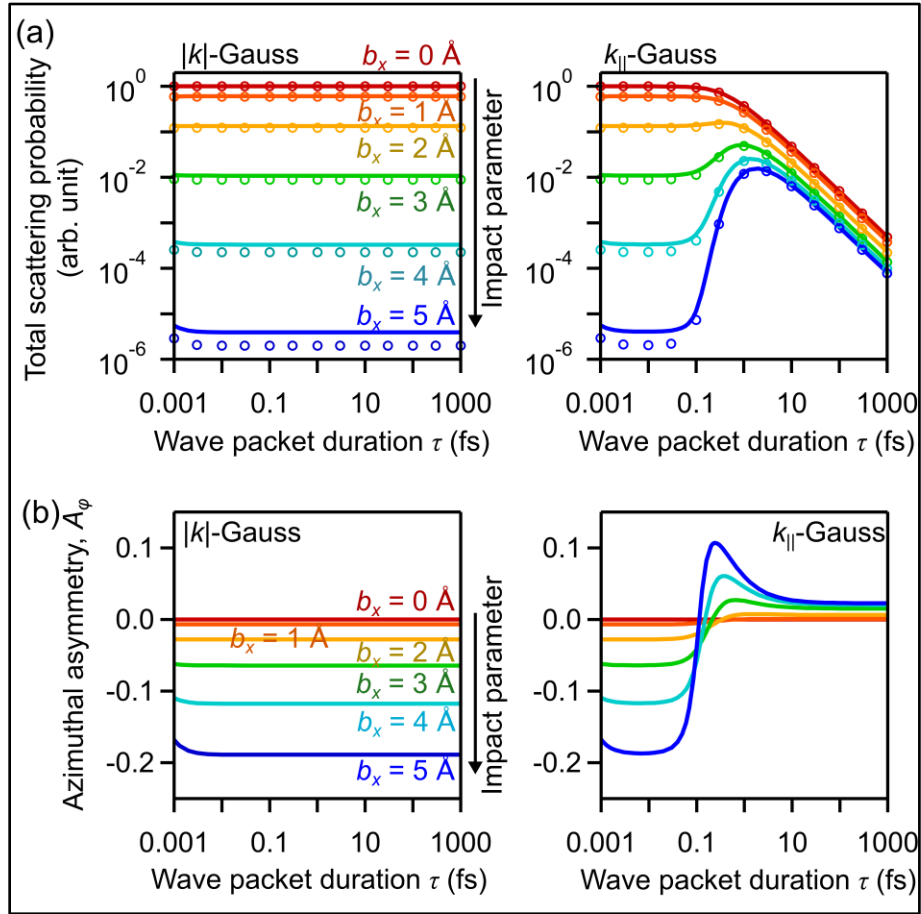


Fig 2. Total scattering probability and azimuthal asymmetry. (a) Total elastic scattering probabilities as a function of the wave packet duration and the impact parameter (solid curves). Wave packet probability densities at the position of the target (circles). (b) Azimuthal asymmetries.

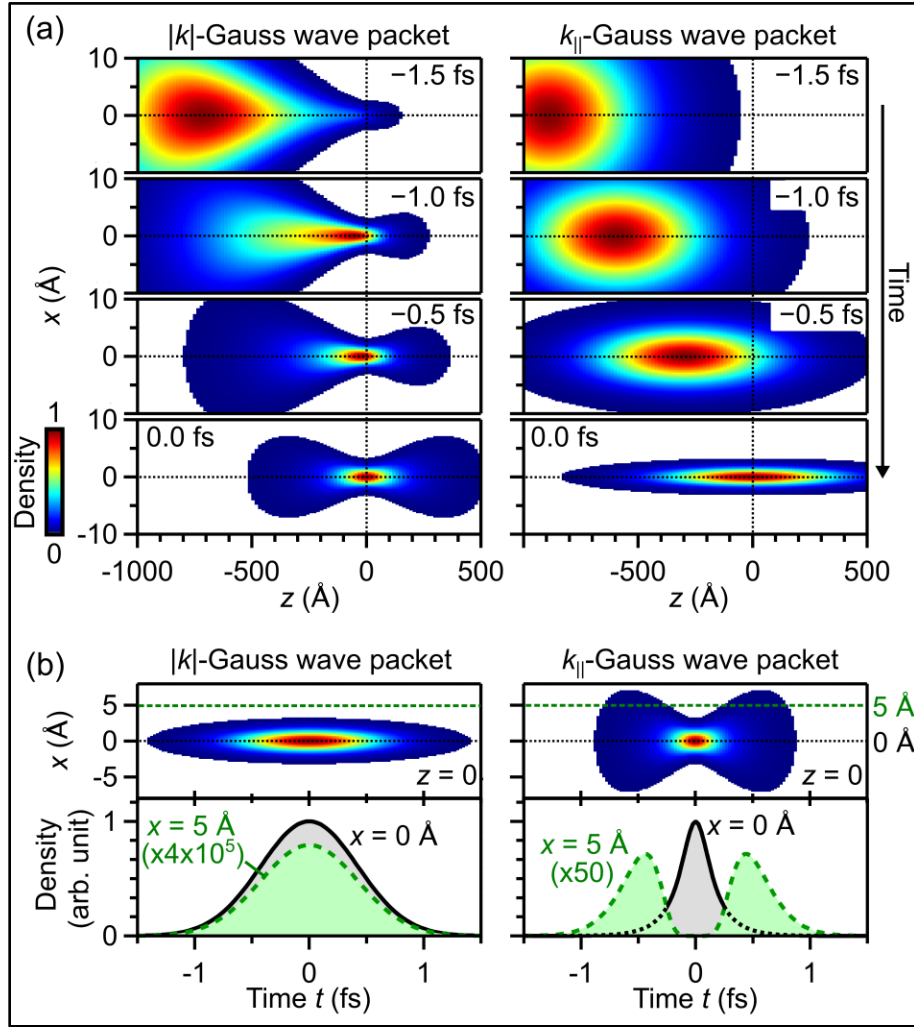


Fig 3. Sub-femtosecond real-space dynamics of the electron wave packets with $\tau = 1$ fs. (a) Snapshots of the wave packets on the xz plane. At time zero (lowest panels), the wave packets are transversally focused. Result of each panel is normalized independently. (b) Upper panels: temporal evolution of the probability densities at $z = 0$. Lower panels: Slices at $x = 0$ and 5 Å.

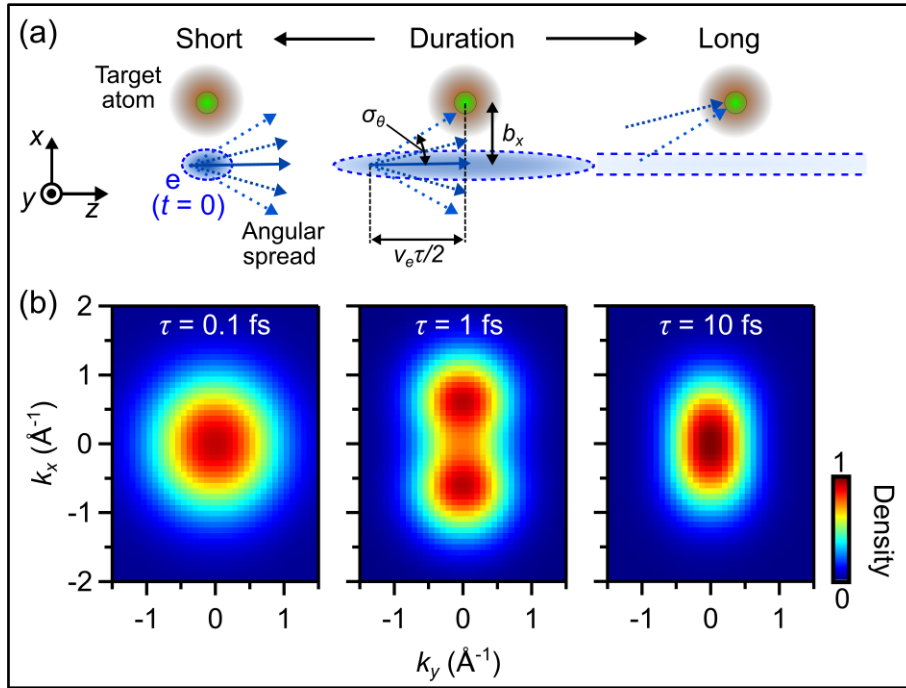


Fig 4. Spatial and momentum overlaps of the $k_{//}$ -Gauss wave packet with a target. (a) Illustration of the wave-packet duration dependence. The FWHM wave-packet longitudinal size is $v_e \tau$. (b) Momentum distribution of the wave packet at the position of the target, given by the Gabor transform, see Eqs. (6)-(7). At the short time duration (left), even a large-angle component cannot reach the target. At the intermediate duration (~ 1 fs), only the large-angle component can reach the target. Accordingly, the momentum distribution is anisotropic. At the long duration (right), components of a wide angular range can reach the target, resulting in a smaller anisotropy.

Supplemental Material

In this supplemental material, we discuss possible experimental schemes based on existing techniques for obtaining the considered wave packets. To achieve packet durations τ below 100 fs, which cannot be directly obtained from ultrashort electron guns [42], a buncher has to be employed, in which a light-driven (green curve in Fig. S1) energy modulation is applied to the incident pulse. Examples of the buncher include a laser-excited thin membrane [17–19,43], a dielectric laser accelerator [23–25] or a two-color ponderomotive potential [22]. The energy modulation at the buncher evolves into the temporal density modulation (i.e., temporal compression) during the subsequent free-space propagation. The $/k/$ -Gauss wave packet has the same energy spectrum over the incident angle θ_i , and therefore, can be produced by a focusing using a magnetic lens (Fig. S1). On the other hand, the $k_{//}$ -Gauss wave packet has a constant longitudinal momentum ($k_{\parallel} = k_i \cos \theta_i$) distribution over θ_i , which corresponds to an energy spectrum whose mean energy increases with the angle θ_i . For example, the component coming with $\theta_i = 10$ mrad has 10^{-4} times higher mean energy (i.e., 10 eV for 10-keV electrons) compared to that of $\theta_i = 0$. To generate such a wave packet, we propose to employ another energy modulator of a thin membrane excited by a THz wave (red curve in Fig. S1) [15,20] whose cycle is longer than the wave packet duration such that a temporally uniform energy modulation (deceleration, here) can be achieved. By setting the electron beam diameter slightly larger than the focused THz beam, electrons experience strongest decelerations at the beam center and reduced deceleration with the distance from the center. Subsequent spatial focusing by a lens produces the $k_{//}$ -Gauss-like wave packet. Alternatively, the space-energy coupled wave packet could be obtained with a dielectric laser accelerator which relies on the spatially-decaying optical near fields and intrinsically provides position-dependent energy modulation amplitude [23–25]. We note that the capability of space-time energy (i.e., wavelength) control with light waves can produce electron wave packets whose analogue are difficult to be achieved with light wave packets.

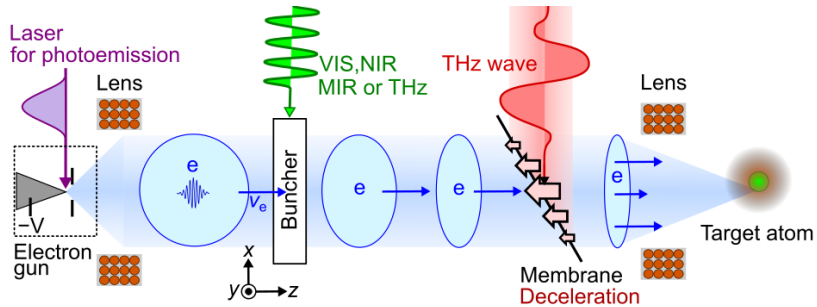


FIG. S1. Proposed scheme for producing $/k/$ -Gauss and $k_{//}$ -Gauss wave packets. A sub-picosecond electron pulse is produced by photoemission triggered by an ultrashort laser pulse (purple). To achieve a duration of <100 fs, a buncher driven by a laser or THz field (green) is employed. A spatially inhomogeneous deceleration by the THz field (red) and the transversal focusing produces the $k_{//}$ -Gauss-like wave packet. The $/k/$ -Gauss-like wave packet is generated without the THz deceleration.